Initial performance metrics of a new custom-designed ArF excimer LA-ICPMS system coupled to a two-volume laser-ablation cell†

Wolfgang Müller,*[a] Michael Shelley,[b] Pascal Miller[c] and Sergey Broude[c]

Received 9th April 2008, Accepted 24th October 2008
First published as an Advance Article on the web 4th December 2008
DOI: 10.1039/b805995k

A new custom-built excimer (193 nm) laser-ablation system with two-volume laser-ablation cell coupled to a quadrupole ICPMS is described, which combines rapid (<1.5 s for 99%) signal washout with full flexibility in sample size (50 × 50 × 25 mm) and high sensitivity (>10000 cps/ppm for mid-high m/z, 55 μm, 5 Hz). An application of reconstructing medieval Pb exposure highlights the need for rapid signal washout in unravelling strongly varying Pb peaks in well-preserved archaeological tooth enamel.

Direct solid sampling by laser-ablation coupled to inductively-coupled-plasma mass spectrometers (LA-ICPMS) has led to an enormous proliferation of *in-situ* elemental and isotopic analyses since the mid-1990s. Emphasis in technique development over the past 10+ years was on reducing laser *wavelength* for improved ablation of IR-transparent materials, such that frequency-multiplied solid-state Nd:YAG lasers at (D)UV wavelengths of 213 nm and more recently 193 nm, as well as gas lasers (excimer) at 193 nm dominate commercially available LA systems. More recently, concomitant reduction in laser *pulse length* from nanosecond to femtosecond duration is being investigated to reduce thermal effects of laser-target interaction.[1]

Despite these laser beam delivery developments, the geometry of the *laser-ablation cell* – where laser-target interaction and transport phenomena occur – has received comparatively little attention with notable exceptions (*e.g.* ref. 2–5), such that commercially available LA systems are equipped with rather unsophisticated LA cells. This is somewhat surprising since right from the outset of laser ablation technique development during the late 1980s, Arrowsmith and Hughes' landmark paper[6] has outlined the key design characteristics of a successful LA cell. The overall conflicting requirements for LA cells imply that cells have to be large enough to enclose variably sized solid samples, while at the same time they must have a small volume to achieve rapid washout and high sensitivity.

Aiming at presenting a laser-ablation system that meets the above LA cell requirements, we introduce a new custom-built ArF excimer (193 nm) laser-ablation system (RESOlution M-50, Resonetics LLC, USA) coupled to a two-volume laser-ablation cell (Laurin Technic, Australia). With modifications, its fundamental design is modelled on the successful excimer-based LA systems at both The Australian National University (ANU)[7,8] and The University of Melbourne,[9,10] in turn based around a mid-1990s Resonetics beam delivery system (BDU) at ANU. At Royal Holloway University of London, the new LA unit is coupled to either an Agilent 7500ce/cs quadrupole ICPMS or an IsoProbe MC-ICPMS, for elemental/low-precision or high-precision isotopic analyses, respectively (Table 1).

The LA cell and BDU design had to meet *all* of the following requirements:

(1) Full flexibility in sample size (50 × 50 mm, 25 mm deep)

(2) Rapid signal washout (less than 1s/order of magnitude)

(3) Invariant gas flow around the ablation site to ensure reproducible elemental and/or isotopic fractionation, irrespective of sample position relative to gas in/outlets

(4) High and uniform sensitivity, irrespective of position in cell

(5) Smooth signals at low laser repetition rates (<5 Hz), important for *e.g.* depth-profiling

(6) Fully computer-controlled X–Y stage movement

(7) No cross contamination of samples in LA cell

These requirements are met in the 'Laurin' LA cell by placing a small (effective volume ~1–2 cm^3), funnel-shaped inner cell, with a hole at the funnel bottom, above a sample holder in a gas tight sample cell box with a volume of 380 cm^3 (Fig. 1). The funnel remains stationary below the imaging lens of the laser beam delivery system, while the sample holder, and thus the entire sample cell box, moves relative to the funnel. This relative movement of funnel and sample holder is made possible by means of a gas-tight corner ball joint, through which the sample aerosol, entrained in a flow of He and collected in the small funnel volume, leaves the cell body through a metal tube. Facilitating transmitted and/or reflected light illumination, the Laurin two-volume laser-ablation cell is cantilevered from the computer-controlled X–Y stage with 50 × 50 mm travel and selectable speed held constant along curved paths. The cell body is capable of holding various sample holders, including four one-inch sample disks or equivalent rectangular samples. Due to the relative movement of sample holder and funnel, samples in the holder are presented beneath a reference surface by being pushed upwards with springs. This has the added benefit that refocusing of the laser and viewing system is unnecessary.

The fully-enclosed and interlocked (laser class 1) laser-ablation system utilizes a water-cooled Compex Pro 110 excimer laser (Coherent; ArF, 193 nm, ~20 ns pulse length) and laser pulses are triggered by the computerized motion controller. The beam delivery system utilizes three 90° turning mirrors contained in a fully N_2-purged optical path to prevent formation of ozone

[a]*Dept. of Earth Sciences, Royal Holloway University of London, Egham, Surrey, TW20 0EX, UK. E-mail: w.muller@es.rhul.ac.uk*
[b]*Laurin Technic P/L., Canberra, ACT 2604, Australia*
[c]*Resonetics LLC, Nashua, NH, 03063, USA*
† Presented at the 2008 Winter Conference on Plasma Spectrochemistry, Temecula, CA, USA, January 7–12, 2008

Table 1 Operating conditions of laser-ablation ICPMS (see text for further details)[a]

ICPMS: Agilent 7500ce/cs	
RF power	1350 W
Sampling depth	6.5 mm
Carrier gas flow (Ar)	approx. 0.65 l/min (optimized daily)
Coolant gas flow	15 l/min
Auxiliary gas flow	1 l/min
Dwell time/mass	20–100 ms
Monitored masses (m/z)	^{25}Mg, ^{43}Ca, ^{65}Cu, ^{66}Zn, ^{88}Sr, ^{138}Ba, ^{140}Ce, ^{175}Lu, ^{205}Tl, ^{208}Pb, ^{209}Bi, ^{232}Th, ^{238}U
Sampler, skimmer cones	Ni
Extraction lenses	ce (mostly); cs
Laser-ablation system RESOlution M-50	
Energy density (fluence) on target	4.0 J/cm^2
ThO^+/Th^+	<0.5%
He gas flow	850 ml/min
N_2 gas flow	4.3 ml/min
Laser repetition rate	variable, 1–15 Hz
Laser spot size	variable, mostly 74 μm
Scan speed (X–Y-stage)	Variable, mostly 1 mm/min
Transport tubing	Nylon, 4 mm diameter; ~5 m length

[a] Data in Fig. 7: concentrations based on stoichiometric Ca in enamel apatite (37 wt%), ^{43}Ca as internal standard, NIST612 as external standard.

and concomitant energy loss on target. The non-homogenized laser beam illuminates either a motorized aperture mask wheel with 12 round apertures producing focused spots on target between 7 and ~350 μm (depending on demagnification) or a variable rectangular aperture (long axis ≤500 μm). Examples of laser craters in NIST 612 and MPI-DING glasses are shown in Fig. 2. Either mask can be positioned at variable demagnifications ranging between 15× and 35×. Energy densities on target range between <3 J/cm^2 to >30 J/cm^2 and are adjustable either via laser energy output and/or the introduction of variable attenuators. Energy densities are uniform across the spot on target and independent of the size or shape of the aperture imaged.

A triplet lens composed of two CaF_2 and one fused silica lenses gives ~128 mm working distance, ~79 mm focal length and depth of focus of ~±0.13 mm and projects the aperture's image onto the sample surface. The long working distance permits the cell window to be 32 mm above the sample surface, which minimizes coating of the window by the expanding plasma plume induced during the laser ablation process. The sample is viewed via an off-axis camera with motorized zoom and focus. In order to visualize the laser spot prior to ablation, the system features a red laser diode whose expanded beam illuminates the aperture. Its image is projected through a pneumatically-activated correction lens onto the sample surface, and produces a well-defined and similarly-sized visible red image of the aperture prior to actual ablation. This is particularly useful on rough sample surfaces.

An automated gas-handling system with mass flow controllers supplies helium (He) to the LA cell. He and the sample aerosol, with Ar carrier gas and optional N_2 as additional di-atomic gas to enhance sensitivity[11] admixed downstream from cell, flows to the (MC-)ICPMS via a smoothing manifold ('squid'). The latter

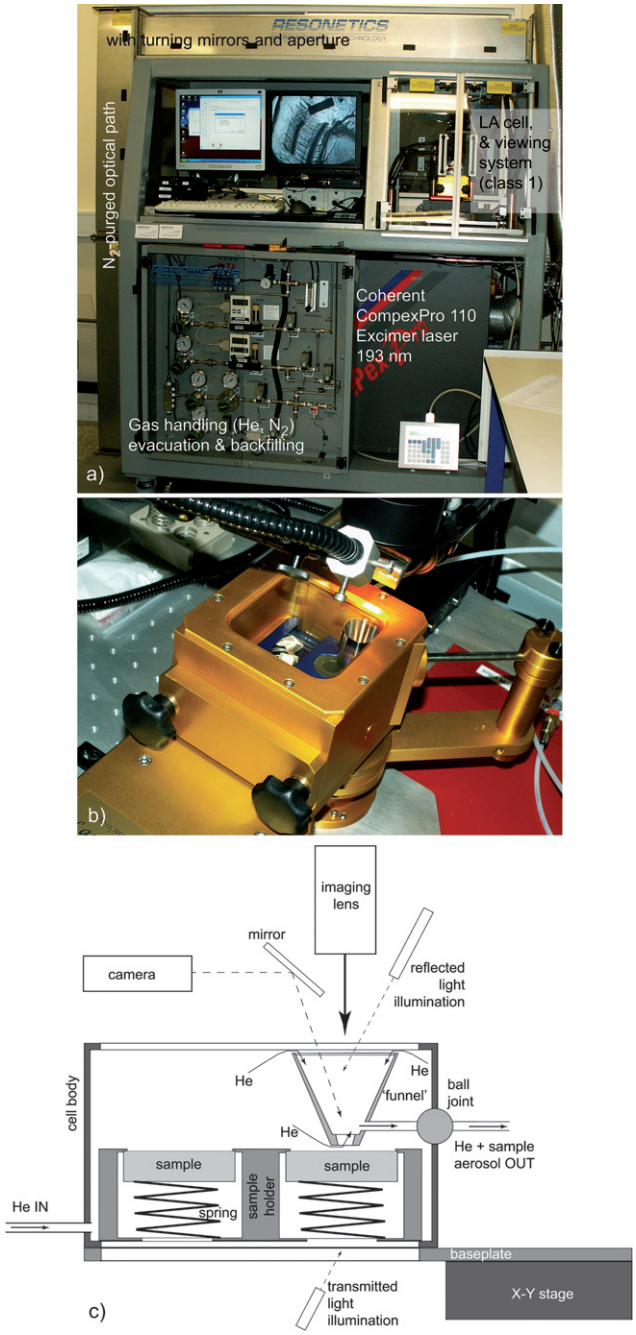

Fig. 1 (a) Photo of laser-ablation unit (ICPMS not visible) showing that the laser beam path is arranged around both excimer laser and ablation cell utilizing three turning mirrors contained in an N_2-purged beam path. (b) Laurin two-volume laser-ablation cell with sample holder and funnel-shaped inner cell. The off-axis camera and mirror as well as reflected light illumination are also visible. (c) Highly schematic cross section of the Laurin two-volume laser-ablation cell (not to scale). Helium (He) enters the cell body at its bottom, and flows from both bottom and top through the funnel, where the He flow entrains the aerosol that condensed out from the laser-induced plasma. Funnel-shaped upper cell and tilted reflected light illumination overall improve the off-axis viewing system. Sample aerosol and He leave the LA cell for the ICPMS via an exit tube connected to the cell body via a ball joint, and Ar and N_2 (optional) are admixed downstream, in front of the 'squid' signal smoothing device. See text for further details.

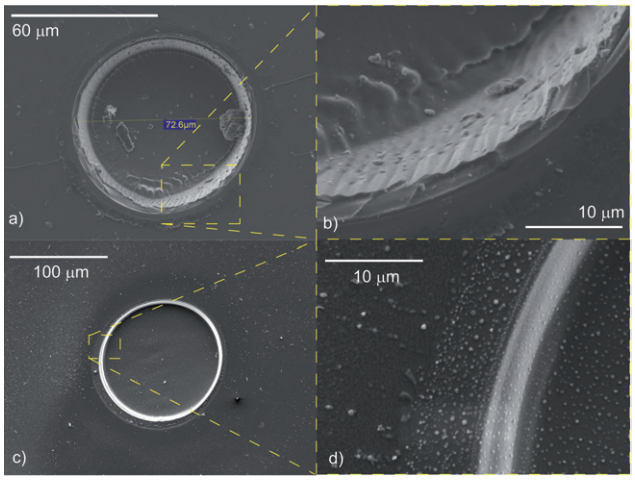

Fig. 2 Selected SEM images: (a) 74 μm laser crater drilled using 225 laser pulses into MPI-DING glass StHs-6/80-G with (b) details of crater wall. (c) 128 μm laser crater in NIST612 glass (50 laser pulses) with (d) crater wall details. Depth-profiles (not shown) reconstructed from stereo-pair SEM imaging show perfectly flat crater geometries.

splits the He + sample aerosol line into ten tubes with optimally differing lengths, such that after recombination into one gas line a smooth signal is produced. Individual gas flow paths have smooth transitions without corners or locations for particle accumulation. Smooth signals are produced even at very low laser repetition rates down to 1 Hz, where the rapid washout of the LA cell otherwise results in pulsed, non-uniform signals. The latter otherwise may lead to undesired beating effects (known also as spectral skew)[12] when choosing certain ICPMS dwell times during data acquisition (*cf.* Fig. 5, 6).

Removal of air from the LA cell after sample exchange is by repeated evacuation and backfilling, using an He-driven venturi pump operated by low-purity He (this avoids air and hydrocarbons backstreaming from a conventional vacuum pump). During this process, the cell gas bypasses the cell and the exit line of the cell is closed off with a pinch valve. Repeated evacuation and backfilling rather than purging with He after sample exchange guarantees complete replacement of air by He, since even trace amounts of air remaining in the cell affect both oxide production and sensitivity of the ICPMS.[11,13]

The operating software allows any operator-selected ablation paths, successions of points or pre-defined tracks to be stored as an ablation sequence, and other key operating parameters like laser energy, repetition rate, X–Y-stage speed, mask size, *etc.* are also software-controlled (a graphical user interface 'Geostar' is being developed). Remote operation, necessary in our case because the MC-ICPMS is located in an adjacent room, is facilitated by a second set of input controls (mouse, keypad, trackball for X–Y stage), with the monitors being able to swivel by 180° to be viewed through a window.

Initial data illustrating the performance of the system are shown in Figs. 3–7. Using a 55 μm spot, 5 Hz laser repetition rate, 1 mm/min scan speed, $ThO^+/Th^+ < 0.5\%$ and U/Th ~ 1, routinely achievable smooth ICPMS signals on NIST 612 for mid and high masses are ≥10000 cps/ppm with an Agilent 7500cs, and approximately half this with ce-lens. Because this preliminary system evaluation focuses on signal stability/homogeneity in the

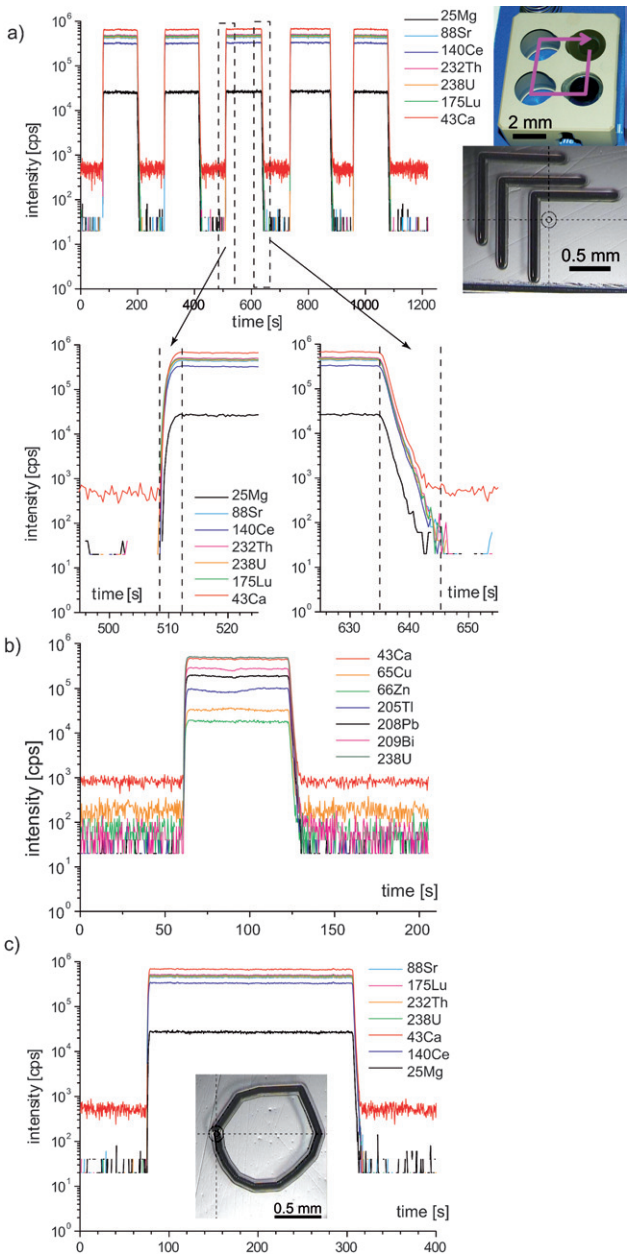

Fig. 3 (a) Raw intensities of seven nuclides in a long-term (~1200 s) stability test of LA-ICPMS signal homogeneity near the four corners of the LA cell, with the squid signal-smoothing device fitted. Each of the five sections is one continuous line scan with a 90° mid-way change in direction on a NIST612 disc at 1 mm/min scan speed. The fifth part closes the square by scanning along the same disc as in the first section (see photographs). Signal washout and rise are shown zoomed-in below. (b) Raw intensities of a shorter scan focusing of five chalcophile nuclides (+ ^{43}Ca and ^{238}U) in NIST612, where homogenously distributed ^{66}Zn shows similar signal smoothness to equally high ^{25}Mg (above), however other nuclides exhibit depletions (^{205}Tl, ^{208}Pb, ^{209}Bi) or enrichments (^{65}Cu) typical of certain zones of NIST612.[14] (c) Continuous line scan along an approximated circle (photograph) showing smooth signals despite frequent changes in scanning direction, revealing invariant gas flow at ablation site. Acquisition parameters (a–c): 10 Hz, 74 μm spot; see text for details.

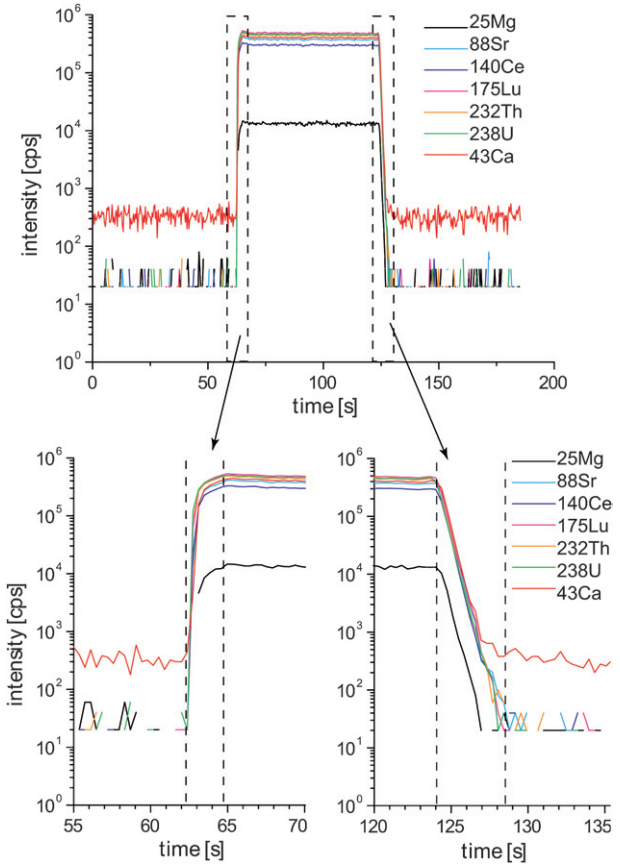

Fig. 4 A similar albeit shorter experiment to Fig. 3 but *without* squid signal-smoothing device. Signal rise and washout are approximately twice as fast; see text for details.

ablation cell as well as on signal washout, data are presented in the form of line scans with and without the smoothing manifold ('squid').

A long-term (~1200 s) stability test of LA-ICPMS signal homogeneity at various positions in the LA cell was conducted. Results of a semi-continuous line scan composed of five 2 mm sections (with a 90° change in scanning direction midway) across four one-inch NIST612 polished discs placed close to the four corners of the LA cell is shown in Fig. 3a. Relative standard deviations (RSD) over ~1200 s for all seven masses (^{25}Mg–^{238}U) range between 2.2–2.4% (3.6% for ^{25}Mg with its lower intensity) and include ICPMS drift (the latter has <3% signal stability specification over 30 min), which is thus judged to be very good. These values are only slightly higher than the internal RSDs (1.3–1.8%; ^{25}Mg: 3.3%) on each of the NIST612 mounts measured for ~120 s, and demonstrate that signal response and sensitivity is homogenous throughout the cell. If ratioed to ^{43}Ca as internal standard to eliminate ICPMS drift, the respective RSDs over 1200 s vary between 1.1–1.2% (2.9% for ^{25}Mg) and 1.0–1.2% on each of the five NIST612 sections. Comparative, yet shorter line scan data of chalcophile elements in NIST612 (Fig. 3b) demonstrate that homogenously distributed ^{66}Zn shows similar signal smoothness to equivalent signal intensities (*e.g.* ^{25}Mg), however other nuclides exhibit depletions (^{205}Tl, ^{209}Bi, ^{208}Pb) or enrichments (^{65}Cu) typical of certain zones of NIST612 (*cf.* ref. 14), thus precluding using those for an assessment of signal stability.

With squid fitted, signal washout over ≥5 orders of magnitude occurs within ~9 s, indicating that 99% signal washout is accomplished within ~3.5 s (Fig. 3a). Corresponding signal rise after switching the laser on is ~3 s for five orders of magnitude. Invariant gas flow characteristics at the ablation site have been evaluated using a continuous line scan along an approximated circle (Fig. 3c). Over the entire ~240 s the relative standard deviations (RSD) for all seven masses (^{25}Mg–^{238}U) range between 1.6–1.7% (3.3% for ^{25}Mg), and 1.1–1.2% (3.1% for ^{25}Mg) if intensities are ratioed to ^{43}Ca, or amongst one another (*e.g.* ^{232}Th/^{238}U).

A shorter stability test *without* squid is shown in Fig. 4, demonstrating the faster washout without signal smoothing. Signal decay takes ~4 s for ≥5 orders of magnitude, and the signal decreases to 1% within ~1.5 s. The corresponding signal rise after switching the laser on is ~2 s.

Signal smoothing and signal stability with increasing laser repetition rates from 1 to 8 Hz are shown in Fig. 5 and 6. Even at the lowest repetition rate of 1 Hz, the squid smoothing device delivers a smooth signal to the ICPMS that is especially crucial for maximum resolution during depth profiling, which is accompanied only by a slight increase in washout (see above). Without smoothing on the other hand, the less than one second washout of the cell results in a strongly pulsed signal at 1 Hz. Signals exhibit pulsing up to 3–5 Hz, which may result in severe beating/resonance effects (spectral skew) depending on the relationship between ICP dwell time and laser repetition rate time, as illustrated in Fig. 6b. Such beating could compromise data, especially when using an internal standard. Thus, below 10 Hz laser repetition rate signal smoothing with the squid is necessary, however, from 10 Hz onwards signal smoothness is fairly similar, with 1–1.5% RSD being routinely achievable for laser scanning over tens of seconds.

The following application of highly-resolved compositional profiling (Fig. 7, Table 1) aims at showcasing the benefits of such a LA cell with rapid washout for accurately revealing extreme compositional changes across short distances. This was encountered in tooth enamel of medieval Pb-Ag miners (Sulzburg, Black Forest, SW Germany, 12th century AD)[15,16] in an attempt to reliably reconstruct past heavy metal exposure. The chosen example is that of a child (S71) who died of bone cancer (osteosarcoma) between age 8–10.[15] Since tooth enamel grows sequentially and does not remineralize after formation, it preserves a time-series of changing environmental parameters that can be revealed using a high-spatial resolution analytical technique such as LA-ICPMS. Enamel grows by ~4 μm per day such that a 20 or 25 μm spot size samples slightly less than one week of enamel growth. The high-density and virtual lack of organic tissue render enamel far less prone to *post-mortem* alteration when compared to dentine or bone,[17] which is crucial for reconstruction of *in-vivo* Pb exposure, since the skeletal material has lain in heavily Pb-polluted soils for centuries such that bones and dentine are strongly contaminated with *post-mortem* added Pb.[16]

Results of selected elements of a full-length continuous compositional scan conducted in the growth direction parallel to the enamel-dentine junction (EDJ) are shown in Fig. 7, panel A. Whereas U and Y are at or below limit of detection (19 and 34 ppb, respectively for the small spots used) indicating pristine

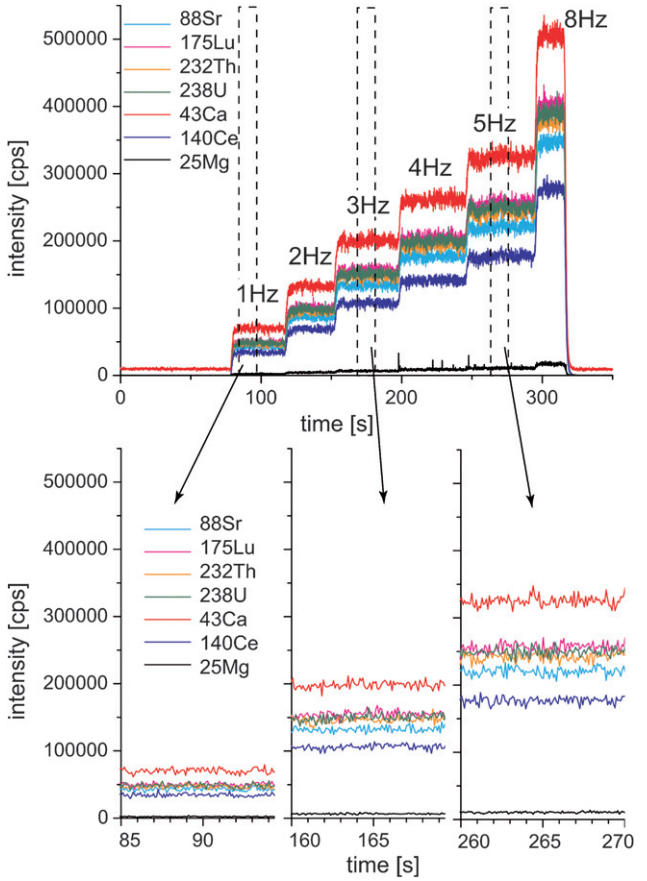

Fig. 5 Experiment exploring the relationship between signal smoothness and increasing laser repetition rates, ranging from 1 to 8 Hz. The lower panel shows ~10 s of the 1, 3 and 5 Hz sections, respectively, and demonstrates smooth signals even for the lowest possible repetition rate of 1 Hz.

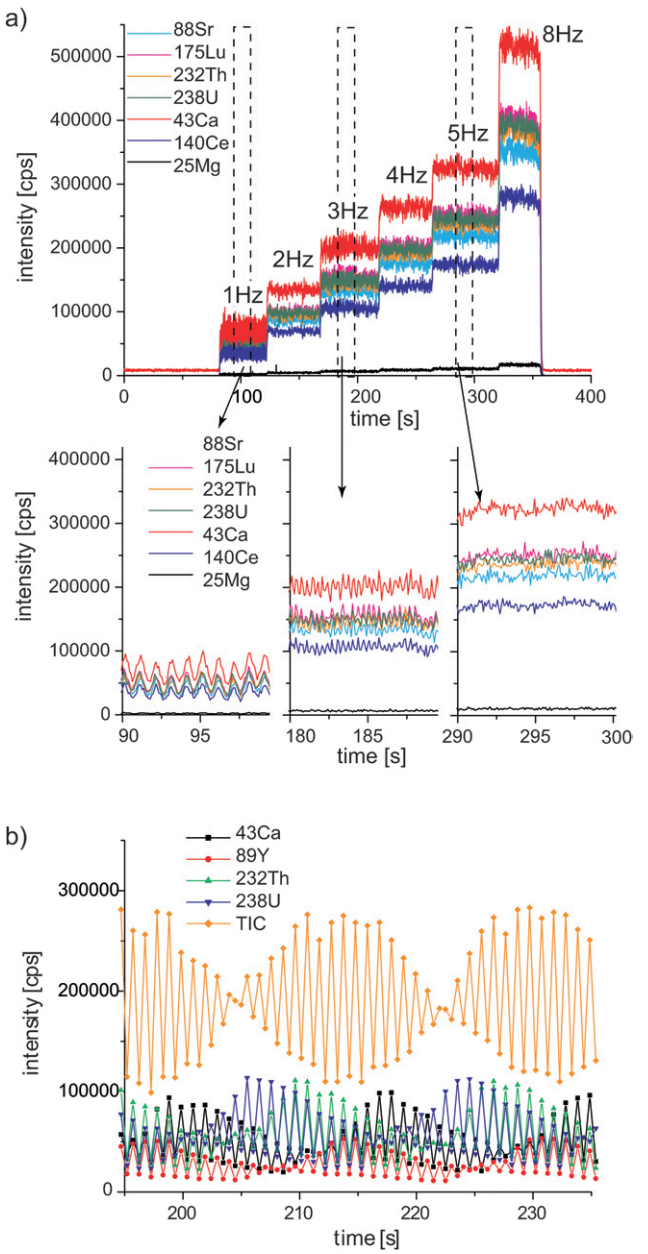

Fig. 6 (a) A similar experiment to Fig. 5 but *without* squid signal-smoothing device. It shows that the LA cell washout of less than 1 s yields a strongly pulsed signal at 1 Hz. Note that beating occurs at 3 Hz for the seven masses sampled at 10 ms dwell time, emphasizing the need for signal smoothing at low laser repetition rates, for example when depth-profiling. (b) Example of the interplay between ICPMS sampling time and laser repetition rate, resulting in severe beating for four nuclides (spectral skew). Internal standardization to *e.g.* ^{43}Ca would lead to strongly varying signals (100 ms dwell time, 1 Hz; TIC = total ion count).

unaltered enamel, strongly variable concentrations are apparent for Pb (and to a lesser degree Ba and Zn). An initial evaluation of the LA-ICPMS results combined with detailed enamel histology[18] (an in-depth analysis is beyond the scope of this paper), reveal several narrow Pb peaks at *e.g.* 4.6, 6.9 and 8.7 mm with very high Pb concentrations (up to 150 ppm Pb), which can be timed to have occurred between yr 1 and 3 (*e.g.* 360, 634, 730 days after birth) by layer-counting from the neonatal line onwards.[19] In contrast, a profile (sub-)parallel to a Retzius line near the 6.9 mm Pb peak (at ~630 days after birth) indicates little change in Pb concentrations (Fig. 7, panel B), apart from the very outer enamel where also modern teeth show characteristic Pb enrichment.[20] Such Retzius lines represent iso-growth lines within enamel and as such the narrow ~100 ppm Pb peak in A appears to be 'frozen' in. On the contrary, the profiles displayed in panels C + D (Fig. 7) were conducted across the enamel parallel to enamel prisms and represent condensed subsections of the entire compositional scan (in A). Profiles were analyzed in opposite directions to evaluate LA cell washout, and even though Pb concentrations vary systematically up to three orders of magnitude across few 100 μm, in both cases the two profiles are perfectly symmetrical, illustrating excellent LA cell washout.

If converted into blood-Pb (PbB) concentrations,[21] such very high and strongly varying Pb concentrations from human enamel are without precedent[22] and yield extremely high peak PbB-values, much in excess of the 80 μg/dl threshold for acute Pb-induced encephalitis.[23] This abundantly demonstrates the power of continuous compositional profiling to capture changing Pb exposure, which in the case of individual S71 may have also

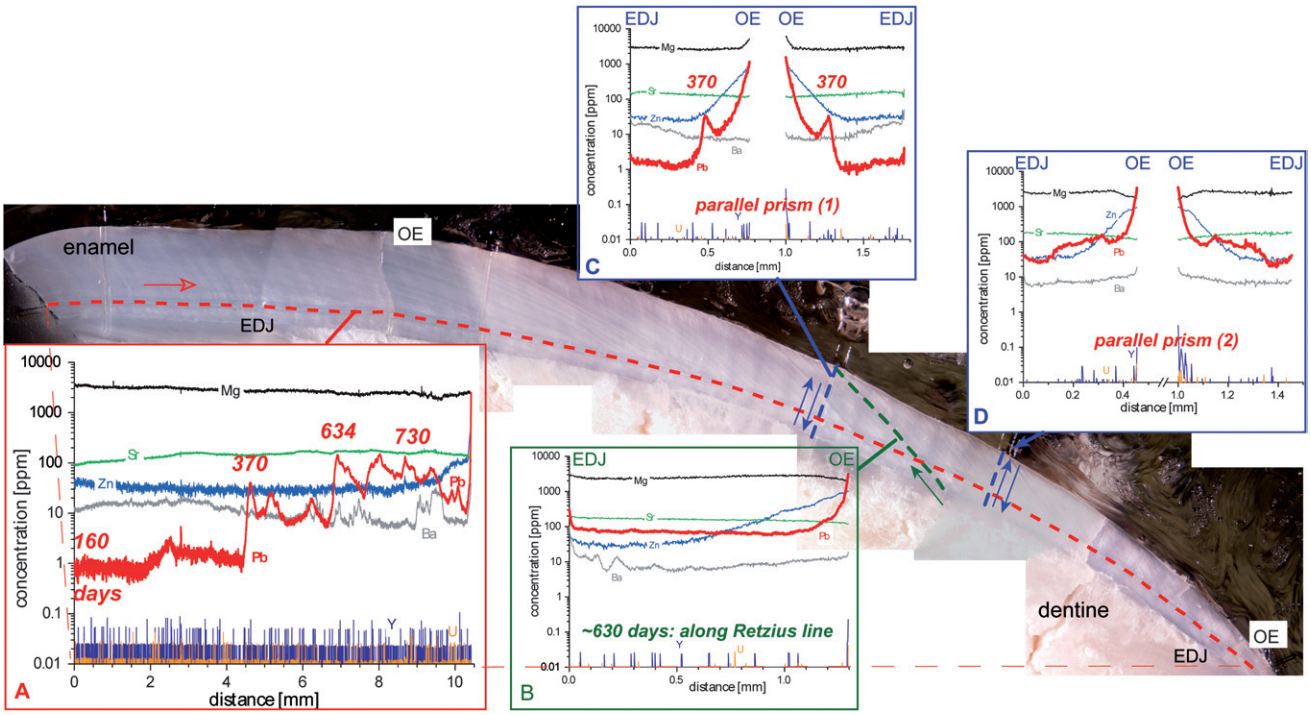

Fig. 7 Composite image of tooth cross section (first permanent incisor; mostly enamel shown) of an 8–10 yr old child from the medieval mining village of Sulzburg, Black Forest, SW Germany; 10–12 century AD). The laser ablation tracks are indicated with dashed lines, and corresponding results are shown in panels A–D (acquisition parameters see Table 1 with the following adjustments: A + B: with 'squid' fitted, 25 μm spot size, 0.5 mm/min scan speed, 15 Hz, 20 ms dwell time for ^{208}Pb; C + D: no 'squid', 20 μm, 0.3 mm/min, 10 Hz, 100 ms dwell time for ^{208}Pb). Arrows indicate profile acquisition directions used, with panels C + D showing the results of scans performed in opposite directions across enamel (parallel to enamel prisms). See text for details (EDJ = enamel-dentine-junction, OE = outer enamel, 370 *etc.* = days after birth).

contributed to the development of bone cancer, given the suspected threshold effect for Pb cancerogenity.[24]

Acknowledgements

Equipment funding by a HEFCE SRIF3 grant at RHUL is acknowledged. Anton Kearsley helped with SEM imaging. Kurt Alt and Luca Bondioli are thanked for discussions about medieval Sulzburg and enamel development, respectively. Comments by three reviewers helped to improve the manuscript. UoL CRF is thanked for co-funding medieval Pb exposure reconstructions.

References

1 I. Horn, F. von Blanckenburg, R. Schoenberg, G. Steinhoefel and G. Markl, *Geochim. Cosmochim. Acta*, 2006, **70**, 3677–3688.
2 D. Bleiner and D. Gunther, *J. Anal. At. Spectrom.*, 2001, **16**, 449–456.
3 T. Hirata, *Anal. Sci.*, 2007, **23**, 1195–1201.
4 E. L. Gurevich and R. Hergenroder, *J. Anal. At. Spectrom.*, 2007, **22**, 1043–1050.
5 D. Autrique, A. Bogaerts, H. Lindner, C. C. Garcia and K. Niemax, *Spectrochim. Acta, Part B*, 2008, **63**, 257–270.
6 P. Arrowsmith and S. K. Hughes, *Appl. Spectrosc.*, 1988, **42**, 1231–1239.
7 S. M. Eggins, L. P. J. Kinsley and J. M. G. Shelley, *Appl. Surf. Sci.*, 1998, **129**, 278–286.
8 S. Eggins, R. Grun, M. T. McCulloch, A. W. G. Pike, J. Chappell and L. Kinsley, *Geochim. Cosmochim. Acta*, 2005, **69**, A377–A377.
9 J. Woodhead, J. Hergt, M. Shelley, S. Eggins and R. Kemp, *Chem. Geol.*, 2004, **209**, 121–135.
10 J. D. Woodhead, J. Hellstrom, J. M. Hergt, A. Greig and R. Maas, *Geostand. Geoanal. Res.*, 2007, **31**, 331–343.
11 S. F. Durrant, *Fresenius J. Anal. Chem.*, 1994, **349**, 768–771.
12 G. D. Schilling, F. J. Andrade, J. H. Barnes, R. P. Sperline, M. B. Denton, C. J. Barinaga, D. W. Koppenaal and G. M. Hieftje, *Anal. Chem.*, 2007, **79**, 7662–7668.
13 R. Kovacs and D. Günther, *J. Anal. At. Spectrom.*, 2008, DOI: 10.1039/b803789b.
14 S. M. Eggins and J. M. G. Shelley, *Geostand. Newsl.*, 2002, **26**, 269–286.
15 K. W. Alt, C. P. Adler, C. H. Buitrago-Tellez and B. Lohrke, *Int. J. Osteoarchaeol.*, 2002, **12**, 442–448.
16 K. W. Alt, B. Lohrke, R. Brenn, W. Müller, M. Rauschkolb and H. Steuer, *Die mittelalterliche Bergbaubevölkerung des 12. Jahrhunderts von Sulzburg, Kr. Breisgau-Hochschwarzwald. Anthropologische und archäometrische Studien*, VML Verlag Leidorf, 2008.
17 P. Budd, J. Montgomery, B. Barreiro and R. G. Thomas, *Appl. Geochem.*, 2000, **15**, 687–694.
18 W. Müller, K. W. Alt, L. Bondioli and B. L. Gulson, *Geochim. Cosmochim. Acta*, 2006, **70**, A436.
19 L. Bondioli and R. Machiarelli, *Am. J. Phys. Anthropol.*, 1999, 94–95.
20 P. Budd, J. Montgomery, A. Cox, P. Krause, B. Barreiro and R. G. Thomas, *Sci. Total Environ.*, 1998, **220**, 121–136.
21 S. R. Grobler, F. S. Theunissen and T. J. V. Kotze, *Archiv. Oral Biol.*, 2000, **45**, 607–609.
22 P. Budd, J. Montgomery, J. Evans and B. Barreiro, *Sci. Total Environ.*, 2000, **263**, 1–10.
23 L. Järup, *Br. Med. Bull.*, 2003, **68**, 167–182.
24 A. Jemal, B. I. Graubard, S. S. Devesa and K. M. Flegal, *Environ. Health Perspect.*, 2002, **110**, 325–329.

